Spin liquid behaviour in $J_{eff} = 1/2$ triangular lattice $Ba_3IrTi_2O_9$

Tusharkanti Dey,[1] A.V. Mahajan,[1,*] P. Khuntia,[2] M. Baenitz,[2] B. Koteswararao,[3] and F.C. Chou[3]

[1]*Department of Physics, Indian Institute of Technology Bombay, Powai, Mumbai 400076, India*
[2]*Max Planck Institute for Chemical Physics of Solids, 01187 Dresden, Germany*
[3]*Center for Condensed Matter Sciences, National Taiwan University, Taipei 10617, Taiwan*

Abstract

$Ba_3IrTi_2O_9$ crystallizes in a hexagonal structure consisting of a layered triangular arrangement of $Ir^{4+}(J_{eff} = 1/2)$. Magnetic susceptibility and heat capacity data show no magnetic ordering down to 0.35 K inspite of a strong magnetic coupling as evidenced by a large Curie-Weiss temperature $\theta_{CW} \sim -130$ K. The magnetic heat capacity follows a power law at low temperature. Our measurements suggest that $Ba_3IrTi_2O_9$ is a 5*d*, Ir-based ($J_{eff} = 1/2$), quantum spin liquid on a 2D triangular lattice.

PACS numbers: 75.40.Cx, 75.45.+j, 75.47.Lx

arXiv:1210.3137v1 [cond-mat.str-el] 11 Oct 2012

Introduction: Since Anderson proposed the resonating valence bond model [1], researchers have been searching for experimental realizations of quantum spin liquids (QSL) [2] in geometrically frustrated magnets. In such materials, incompatibility of local interactions, called frustration, leads to a strong enhancement of quantum spin fluctuations and effectively suppresses the long range magnetic ordering. As a result, the material remains paramagnetic down to very low temperature compared to the Curie-Weiss (CW) temperature θ_{CW}. The frustration in these materials often arises from some special geometries like triangular, kagomé, pyrochlore, garnet etc. [3].

The spin liquid candidates found so far have been mostly 3*d* transition metal based materials. A few examples are two-dimensional (2D) Kagomé systems $SrCr_{9p}Ga_{12-9p}O_{19}$ ($S = 3/2$) [4], and $ZnCu_3(OH)_6Cl_2$ ($S = 1/2$) [5], $S = 1$ 2D triangular lattice antiferromagnet $NiGa_2S_4$ [6], organic materials like $S = 1/2$ triangular lattice κ-$(ET)_2Cu_2(CN)_3$ [7] etc. There are very few examples of spin liquid systems with 4*d* or 5*d* spins. $Na_4Ir_3O_8$ [8], a $S = 1/2$ spin liquid in a three-dimensional (3D) hyperkagome network, is probably the most notable member of the 5*d* spin liquid family.

Recently, $Ba_3CuSb_2O_9$ ($S = 1/2$) with hexagonal space group $P6_3mc$ was suggested to be in the QSL ground state [9]. High pressure hexagonal ($P6_3mc$, 6H-B) and cubic (Fm-3m, 3C) phases of $Ba_3NiSb_2O_9$ have also been suggested to be in the 2D and 3D QSL ground state, respectively [10].

We have been searching for QSL candidates among hexagonal oxides with 4*d*/5*d* elements instead of 3*d* elements. The 5*d* materials are very different from 3*d* materials and thus interesting because of a weak onsite Coulomb energy but a strong spin-orbit coupling. For example, Sr_2IrO_4 [11] and Ba_2IrO_4 [12] are reported to be spin-orbit driven Mott insulators. The magnetic properties of these systems have been described based on a $J_{eff} = 1/2$ state for the Ir^{4+} ion. Among the various Ir-based compounds, $Ba_3IrTi_2O_9$ is rather interesting since it has a chemical formula similar to the Cu and Ni-based compounds (discussed in the previous paragraph) and it crystallizes in a hexagonal structure [13]. However, detailed structural parameters have not been reported. Bryne *et al.* [13] reported magnetic susceptibility of $Ba_3IrTi_2O_9$ in the temperature range $77 - 600$ K. High antiferromagnetic Weiss temperature ($\mid \theta_{CW} \mid > 400$ K) was obtained by them, suggesting that the magnetic Ir^{4+} ions are strongly coupled with each other. An obvious question arises, do they order at lower temperatures? If not then, is it a spin liquid system and a 5*d* analog of $Ba_3CuSb_2O_9$?

Here we report preparation, structural analysis, magnetic susceptibility and specific heat measurements on $Ba_3IrTi_2O_9$. It crystallizes in space group $P6_3mc$ like $Ba_3CuSb_2O_9$ and 6H-B phase of $Ba_3NiSb_2O_9$. A large negative θ_{CW} is obtained from CW fitting of susceptibility data but no magnetic ordering is found from susceptibility and heat capacity measurements down to 0.35 K. Magnetic heat capacity follows a power law at low temperature. This indicates that the system is highly frustrated and an example of a 5*d* QSL. We suggest that this is the first candidate of a 5*d* based quantum spin liquid on a 2D triangular lattice with $J_{eff} = 1/2$.

Experimental Details: Polycrystalline sample of $Ba_3IrTi_2O_9$ was prepared by conventional solid state reaction method using high purity (99.9%) starting materials.

Powder x-ray diffraction (XRD) measurements were performed at room temperature with Cu K_α radiation ($\lambda = 1.54182$Å) in a PANalytical X'Pert PRO diffractometer. Magnetization measurements were performed in a Quantum Design SQUID Vibrating Sample Magnetometer (SVSM). Heat capacity measurements were carried out in the temperature range $0.35 - 295$ K and field range $0 - 9$ T in a Quantum Design Physical Properties Measurement System (PPMS). High temperature (upto 800 K) susceptibility was measured using a PPMS VSM.

Results and Discussions: XRD measurement was done to check the phase purity of the sample and to de-

*Email: mahajan@phy.iitb.ac.in

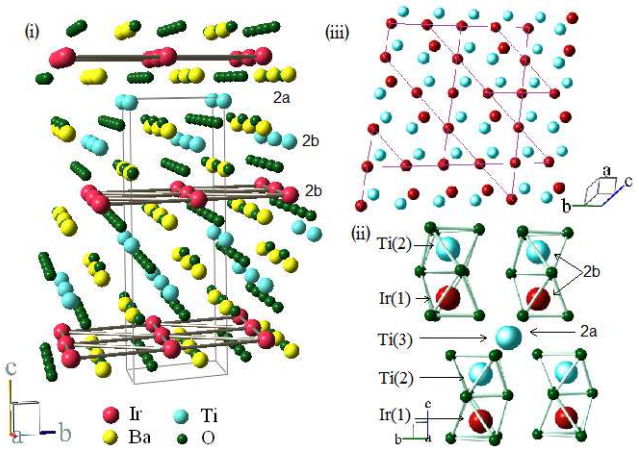

Figure 1: (i) Structure of $Ba_3IrTi_2O_9$ without any site disorder between Ti^{4+} and Ir^{4+}. The triangular arrangement of Ir^{4+} spins in the *ab* plane is shown (ii) $IrTiO_9$ dimers are shown (iii) One possible arrangement of Ti^{4+} and Ir^{4+} ions in the *ab* plane is shown when about 1/3 of Ir^{4+} ions from Ir(1) site are exchanged with Ti^{4+} ions of the Ti(2) site.

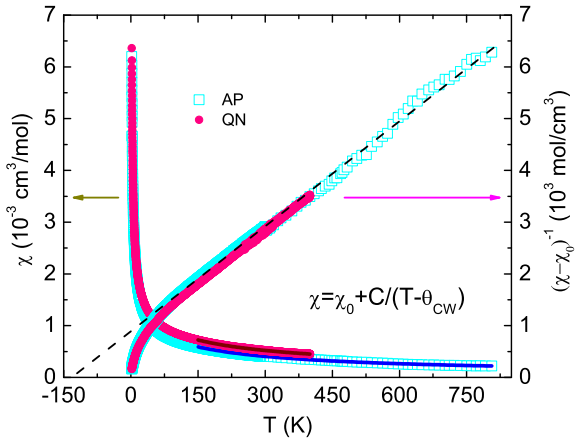

Figure 2: Left axis: Magnetic susceptibilities of as prepared (AP) and quenched (QN) $Ba_3IrTi_2O_9$ samples are shown. Solid lines denote fitting with CW law in high temperature range > 150 K. Right axis: Inverse susceptibilities (after subtracting χ_0) as function of temperature for both AP and QN. The dashed line is a linear extrapolation of high temperature data of AP sample.

termine crystal parameters, as the parameters were not mentioned in the earlier report [13]. The Ru-analog of $Ba_3IrTi_2O_9$ i.e., $Ba_3RuTi_2O_9$ has been mentioned in literature and it crystallizes in the hexagonal $P6_3mc$ space group [14]. On the other hand, with a different Ir and Ti ratio, $Ba_3TiIr_2O_9$ has been suggested to crystallize in the space group $P6_3/mmc$ [15]. In both these space groups metal-metal structural dimers (2b sites or 4f site) are separated by the 2a site metal plane. In $P6_3mc$, the metal ions within the dimer are ordered while in $P6_3/mmc$ space group the metal ions within the dimers are not ordered. We tried to refine our XRD data using these space groups and found $P6_3mc$ gives better refinement with a large site sharing by the Ti^{4+} and Ir^{4+} ions (see supplemental material [16]). The lattice constants obtained from refinement are $a = b = 5.7214$Å and $c = 14.0721$Å.

In the ideal case (i.e., without any site disorder), the Ti(3) site is occupied by Ti^{4+} ions and the Ti(2) and Ir(1) sites are occupied by distinct metal ions Ti^{4+} and Ir^{4+} ions, respectively. This is indeed (nearly) the situation in $Ba_3CuSb_2O_9$ where the Cu site is occupied only by Cu^{2+} (leaving aside a 5% site disorder), and Sb^{5+} ions are located at Sb(1) and Sb(2) sites. However in our case, we found a $(37\pm10)\%$ site sharing of Ir^{4+} ions with Ti^{4+} ions between Ir(1) and Ti(2) sites and $(7 \pm 4)\%$ site sharing with Ti^{4+} ions in Ti(3) site. This is in fact not unexpected, as their ionic radii are very similar. Sakamoto *et al.* also found 21% site sharing between Ti^{4+} and Ir^{4+} in $Ba_3TiIr_2O_9$ [15] and a similar site disordered situation is reported in the case of $Ba_3RuTi_2O_9$ by Radtke *et al.* [17]. They studied probability of different Ru^{4+} and Ti^{4+} combinations based on high resolution electron energy loss spectroscopy and first principles band structure calculations and concluded that site sharing of ions in 2b sites (i.e., Ir(1) and Ti(2) sites in our case) is more probable while site sharing with 2a sites (i.e., Ir(1) and Ti(3) sites in our case) is less probable. This was suggested because structural dimers of like ions (Ti-Ti) are energetically unfavourable due to a strong Ti-Ti repulsion. The same reason is probably valid in our case and results in a small 7% site sharing between Ir^{4+} ions at Ir(1) site and Ti^{4+} ions at Ti(3) site.

In case of perfect ordering among Ti^{4+} and Ir^{4+}, these two ions form face-sharing $IrTiO_9$ bioctahedra (shown in Fig. 1(ii)) and Ir^{4+} spins form an edge-shared triangular lattice in the *ab* plane, as shown in Fig. 1. As a consequence of site disorder, the edge-shared triangular planes will be depleted. Further, Ir occupying the Ti(2) sites might also form a depleted triangular plane. A possible arrangement is shown in Fig. 1(iii). The blue atoms represent Ti and the red atoms are Ir.

Zero field cooled (ZFC) and field cooled (FC) magnetic susceptibility was measured with different fields in the temperature range $2 - 400$ K. No magnetic ordering is found down to 2 K but with 100 Oe field ZFC-FC splitting is seen below 80 K (shown in Fig. [8] in supplemental material [16]). However, the splitting is very small (only 11% of total magnetization at 2 K) and supressed when measured even with 500 Oe. This suggests that a small fraction of the spins take part in a glassy state while the majority of the spins do not. In $Na_4Ir_3O_8$ also a small ZFC-FC ($< 10\%$ of total magnetization) splitting was observed below 6 K which the authors concluded as coming from a small fraction of the spins [8]. Fig. 2 shows the temperature (T) dependence of dc magnetic susceptibility of the as-prepared sample (light-blue open squares). Data obtained with field 5 kOe using a SVSM

(2 − 300 K) and using a VSM with a high-temperature attachment with field 50 kOe (300 − 800 K) have been shown together. Susceptibility data can be fitted well with the CW formula in the high temperature (150 − 800 K) region (shown in Fig. 2), which yields temperature independent susceptibility $\chi_0 = 0.61 \times 10^{-4}$ cm^3/mol, Curie constant $C = 0.149$ cm^3 K/mol and $\theta_{\rm CW} = -133$ K. In many Ir based oxides χ_0 is found to be large and varies within a wide range [15, 18]. The C value obtained from fitting is much less than that expected for $S = 1/2$ magnetic moments (0.375 cm^3 K/mol) value. The large $\theta_{\rm CW}$ value suggests that there still are significant correlations in the triangular planes despite the depletion. The suppression of magnetic moments could be an effect of the extended nature of the 5d orbitals and the strong spin-orbit coupling expected for 5d transition metal oxides. Indeed, in the magnetically ordered iridates such as Sr_2IrO_4 the low temperature saturation moments have been found to be less than one tenth of a $\mu_{\rm B}$ and effective moment in the paramagnetic region is found to be $\sim 0.4\mu_{\rm B}$ [19].

With the aim of investigating as to how the preparation procedure might affect the site ordering and hence the magnetic properties, we quenched the as-prepared sample in liquid nitrogen from 1000^{0}C. Comparing the normalised x-ray diffraction pattern of both as-prepared (AP) and quenched (QN) samples, we found that width of all the peaks and peak height of many peaks are decreased in the QN sample. This indicates that the crystal symmetry is unchanged but ionic disorder (and possibly distortions) are less in the QN sample compared to the AP sample. Refinement of XRD pattern is consistent with a $\sim 35\%$ site disorder between Ir^{4+} and Ti^{4+} cations at the 2b site but without any site sharing with the 2a site Ti^{4+} cations. We also found a marginal increase in the lattice constants with $a = b = 5.7216$Å and $c = 14.0768$Å. Susceptibility for the QN sample measured with field 5 kOe in the temperature range 2 − 400 K (Fig. 2) shows no sign of magnetic ordering. Data fitted to CW law in the temperature range (150 − 400 K) yields $\chi_0 = 1.68 \times 10^{-4}$ cm^3/mol, $C = 0.145$ cm^3 K/mol and $\theta_{\rm CW} = -111$ K. The $\theta_{\rm CW}$ is somewhat smaller than in the AP sample while C is nearly unchanged. Inverse susceptibilities (after subtracting the temperature independent part χ_0) of AP and QN samples are linear in temperature and deviate from linearity below ~ 80 K, as shown on the right axis of Fig. 2.

The large, negative $\theta_{\rm CW}$ indicates that Ir^{4+} magnetic moments are strongly antiferromagnetically coupled with each other. Apparently something prevents long range magnetic ordering to set in even at 0.35 K (evident from heat capacity measurement) which is nearly four hundred times lower than $\theta_{\rm CW}$. This suggests that inspite of the depletion of magnetic ions from the triangular planes, geometrical frustration continues to exist in the depleted triangular lattice and plays a dominant role in determining the magnetic properties of this system. Note that a part of the Curie term could be arising from a few percent of uncorrelated Ir^{4+} spins (and possibly some Ti^{3+} as well) present in the system, which we call orphan spins (discussed later).

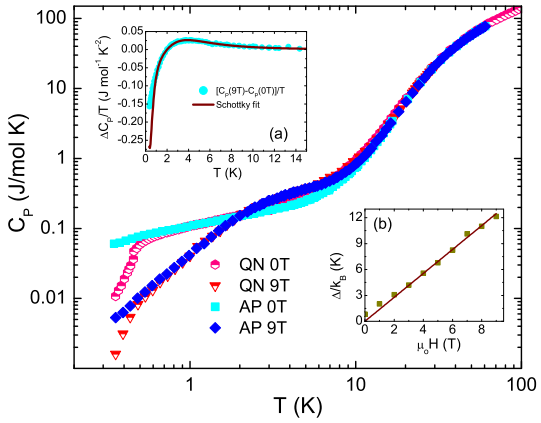

Figure 3: Heat capacity of AP and QN $Ba_3IrTi_2O_9$ sample measured in various applied magnetic fields are shown in a log-log scale. Inset: (a) Solid circles represent $[C_{\rm P}(9\,{\rm T})$-$C_{\rm P}(0\,{\rm T})]/T$ of the AP sample and the solid line is the fit (see the text). (b) Δ/k_B as a function of μ_0H from 0T to 9T is shown and the solid line is a fit to Zeeman splitting.

One should note that in literature $\mid \theta_{\rm CW} \mid$ and μ_{eff} reported for $Ba_3IrTi_2O_9$ are greater than 400 K and $1.73\mu_{\rm B}$, respectively [13] which are at variance from our data. To clarify this discrepancy, we have fitted the published data (Fig. [9] in supplemental material [16]) with CW law and found $\chi_{0\rm B} = 3.42 \times 10^{-4}$ cm^3/mol, $C = 0.10$ cm^{3}K/mol ($\mu_{eff} = 0.89\mu_B$) and $\theta_{\rm CW} = -104$ K. Apparently, Bryne *et al.* used $\chi_{0\rm A} = 0.5 \times 10^{-4}$ cm^3/mol leading them to infer a different $\theta_{\rm CW}$ and μ_{eff} (see supplemental material [16] for details).

Next, in Fig. 3 we present the heat capacity ($C_{\rm P}$) in various fields for the AP and QN samples (data for all fields are shown in supplemental material [16]). No anomaly indicative of long range ordering is found in the measurement range (0.35 − 295 K). For both the samples, $C_{\rm P}$ depends on the applied field below ~ 20 K. This field dependence could be arising from a Schottky anomaly of orphan spins. We model the heat capacity of $Ba_3IrTi_2O_9$ as arising out of four contributions. These are namely, the magnetic contribution of the correlated spins ($C_{\rm M}$), the lattice contribution ($C_{\rm lat}$) and the Schottky anomaly of the orphan spins ($C_{\rm Sch-orp}$) and the nuclear Schottky anomaly.

To extract the magnetic part of the heat capacity arising from correlated magnetic moments, we proceed as follows. The $C_{\rm P}$ has contributions from $C_{\rm M}$, $C_{\rm lat}$, the Schottky anomaly ($C_{\rm Sch-orp}$) from Ir orphan spins and nuclear Schottky anomaly ($C_{\rm Sch-nuc}$). $C_{\rm lat}$ is field independent while the others might be field dependent. Using the zero field heat capacity $[C_{\rm P}(0\,{\rm T})]$ and that measured with 'nT' field $[C_{\rm P}({\rm nT})]$, we obtain

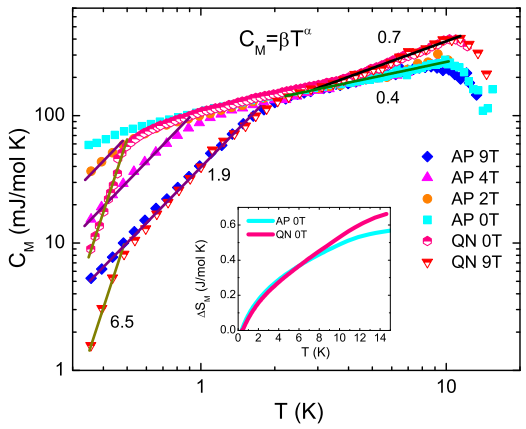

Figure 4: Magnetic heat capacity for the AP and the QN samples are shown. The solid lines are fit to power law with power indicated in the figure. In the low temperature region, solid lines with similar color are with same power. Inset: Magnetic entropy change $\triangle S_M$ is shown as a function of temperature for 0T.

$\Delta C_{\rm P-Ir}/T = [C_{\rm P}(\rm n\,T)\text{-}C_{\rm P}(0\,\rm T)]/T$. This is then fitted with $f[C_{\rm Sch}(\Delta_1) - C_{\rm Sch}(\Delta_2)]/T$, where f is the percentage of orphan spins present in the sample. $C_{\rm Sch}(\Delta_1)$, and $C_{\rm Sch}(\Delta_2)$ are the Schottky anomalies from $S = 1/2$ spins and Δ_1 and Δ_2 are the level splittings with applied magnetic fields H_1 and H_2, respectively. Here,

$$C_{\rm Sch}(\Delta) = R\left(\frac{\Delta}{k_B T}\right)^2 \frac{exp\left(\frac{\Delta}{k_B T}\right)}{\left[1 + exp\left(\frac{\Delta}{k_B T}\right)\right]^2} \qquad (1)$$

where R is the universal gas constant and k_B is the Boltzman constant. Inset (a) of Fig. 3 shows $\Delta C_{\rm P-Ir}/T$ obtained for 0T and 9T along with the fit described above. The good fit above $\sim 2\,$K suggests that $C_{\rm M}$ is not field dependent at least above $\sim 2\,$K and all the field dependence is in $C_{\rm Sch-orp}$. However, below $\sim 2\,$K, there is deviation of the fit from the data (this is much larger than the expected nuclear Schottky anomaly) which suggests the $C_{\rm M}$ might be field dependent there. The fraction of orphan spins f is found to be $\sim 3\%$. The Schottky splitting (Δ/k_B) obtained from fitting for different fields is plotted as a function of field in the inset (b) of Fig. 3. Similar analysis has been reported for $Ba_3CuSb_2O_9$ [9], $ZnCu_3(OH)_6Cl_2$ [20], Y_2BaNiO_5 [21] etc. At zero field also we found a level splitting of $1.8\,$K which is unexpected but found in $Ba_3CuSb_2O_9$ [9] as well. For $\mu_0 H \geq 2$T, the Schottky splitting gap follows $\Delta = g\mu_B H$, as expected for free spin Schottky anomalies. The 'g' value for orphan spins obtained from the linear fit is 2.06.

Using Eq. 1, the Schottky heat capacity can now be subtracted from the measured heat capacity of $Ba_3IrTi_2O_9$. Next, we would like to extract the lattice heat capacity and for that we have used $Ba_3ZnSb_2O_9$ as non-magnetic analog. Since the Debye frequency is primarily determined by the lighter atoms (in these cases oxygens), it will not vary much between these two. The high-temperature heat capacities of $Ba_3IrTi_2O_9$ and $Ba_3ZnSb_2O_9$ differ because of the difference in their molecular weights and lattice volume. By scaling the heat capacity of $Ba_3ZnSb_2O_9$ (obtained from Ref. [9]) by a factor of ~ 0.75 we find that the heat capacities of $Ba_3ZnSb_2O_9$ and $Ba_3IrTi_2O_9$ match in the temperature region $\sim 20\,$K-$30\,$K. The scaled heat capacity of $Ba_3ZnSb_2O_9$ is then subtracted from that of $Ba_3IrTi_2O_9$ in order to obtain the magnetic heat capacity as shown in Fig. 4.

The $C_{\rm M}$ for both AP and QN samples is independent of field from ~ 2.5-$10\,$K and in this range they follow a power law in temperature with power ~ 0.4 for the AP sample and ~ 0.7 for the QN sample. Above $\sim 10\,$K the results can be largely affected by uncertainties associated with the subtraction process. Notably, $C_{\rm M}$ for the QN sample is larger than that for the AP sample. Below $\sim 2\,$K, $C_{\rm M}$ becomes field dependent (for both samples) but follows a power law with temperature with the same power for different fields. This power is 1.9 for the AP sample and 6.5 for the QN sample at very low temperature (shown in Fig. 4). From the heat capacity data of $Ba_3CuSb_2O_9$ (with space group $P6_3/mmc$) published in Ref. [22], we have extracted $C_{\rm M}$ by subtracting a Schottky contribution. Here also we found $C_{\rm M}$ to be field dependent below $\sim 2\,$K but following a power law with power 2.1 for different fields and field independent in the rage $5 - 15\,$K (see supplemental material [16]). In many other frustrated systems $C_{\rm M}$ follows a power law with temperature. The power is 2 for the 2D $S = 1$ system $NiGa_2S_4$ [6], 1 and 2 for $Ba_3NiSb_2O_9$ 6H-B and 3C phases respectively, between 2 and 3 for $Na_4Ir_3O_8$ [8] and 1 at low-temperature but 2 at higher temperature in $S = 1/2$ system $Ba_3CuSb_2O_9$ (with space group $P6_3mc$) [9]. A power of 2/3 was predicted by Motrunich [23] for $S = 1/2$ triangular lattice organic spin liquid system κ-$(ET)_2Cu_2(CN)_3$. In view of the fact that our Ir-based system is expected to have a significant spin-orbit coupling, a fresh theoretical effort in this direction is warranted.

Magnetic entropy change $(\triangle S_{\rm M})$ is obtained by integration of $C_{\rm M}/T$ with T and is shown as a function of temperature in the inset of Fig. 4. The $\triangle S_{\rm M}$ is an order of magnitude lower than $R\ln 2$ expected for ordered $S = 1/2$ systems. In many geometrically frustrated systems it is observed that the entropy change is lower than expected value. For example, the entropy change is 30% and 41% of $R\ln(2S + 1)$ for $Ba_3CuSb_2O_9$ and $Ba_3NiSb_2O_9$ (6H-B phase) respectively, which are similar in structure with $Ba_3IrTi_2O_9$. However, in $Ba_3IrTi_2O_9$ the magnetic moments are strongly reduced probably due to a strong spin-orbit coupling. Here S is not a good quantum number and probably J_{eff} is. So the expected

entropy change may not be $R\ln(2S+1)$ i.e $R\ln 2$, but rather a much smaller quantity. Interestingly, the heat capacity is different for the QN sample compared to the AP sample implying the influence of atomic site disorder on the details of the triangular lattice and hence the ground state.

Conclusions: We have presented a potentially new spin liquid system $Ba_3IrTi_2O_9$ which is based on a triangular lattice of Ir^{4+} ions with electrons responsible for the magnetic properties coming from the $5d$ electronic orbital. The sample crystallizes in $P6_3mc$ space group with a large disorder between Ti^{4+} and Ir^{4+} cations resulting in a site dilution of nearly 1/3 of the Ir^{4+} sites of the edge-shared triangular plane by non-magnetic Ti^{4+}. Apparently, magnetic correlations and frustrations are still maintained with the absence of magnetic ordering down to 0.35 K inspite of a high $\theta_{\rm CW}$ value (~ -130 K). Associated with this is a magnetic heat capacity which, though field dependent, follows a power law with power 1.9 in the low-temperature range. The QN sample has a different behavior. This is somewhat like in $Ba_3CuSb_2O_9$ where different atomic arrangements (Ref. [9] and Ref. [22]) give rise to different magnetic heat capacity. As Nakatsuji *et al.* [22] has reported that due to site sharing between Cu^{2+} and Sb^{5+} ions, a distorted honeycomb lattice is formed in $Ba_3CuSb_2O_9$, we speculate that a similar situation may occur in $Ba_3IrTi_2O_9$ yet maintaining a spin liquid ground state. With the demonstration of the existence of a $J_{eff} = 1/2$ state (having a large spin-orbit coupling) in Sr_2IrO_4 [24], $Ba_3IrTi_2O_9$ is possibly an example of a $J_{eff} = 1/2$ quantum spin liquid system and a $5d$ analog of $Ba_3CuSb_2O_9$. This should open up a new area pertinent to the search for exotic magnetic behaviour in $5d$ transition metal based compounds.

Acknowledgement: We thank Department of Science and Technology, Govt. of India for financial support. FCC acknowledges the support from National Science Council of Taiwan under project number NSC-100-2119-M-002-021.

[1] P.W. Anderson, Mater. Res. Bull. **8**, 153 (1973)
[2] L. Balents, Nature (London) **464**, 199 (2010)
[3] For a review, see Introduction to Frustrated Magnetism, edited by C. Lacroix, P. Mendels, F. Mila, Springer, Heidelberg (2010)
[4] A. P. Ramirez, B. Hessen, and M.Winklemann, Phys. Rev. Lett. **84**, 2957 (2000)
[5] J. S. Helton, K. Matan, M. P. Shores, E. A. Nytko, B. M. Bartlett, Y. Yoshida, Y. Takano, A. Suslov, Y. Qiu, J.-H. Chung, D. G. Nocera, and Y. S. Lee, Phys. Rev. Lett. **98**, 107204 (2007)
[6] S. Nakatsuji, Y. Nambu, H. Tonomura, O. Sakai, S. Jonas, C. Broholm, H. Tsunetsugu, Y. Qiu, and Y. Maeno, Science **309**, 1697 (2005)
[7] Y. Shimizu, K. Miyagawa, K. Kanoda, M. Maesato, and G. Saito, Phys. Rev. Lett. **91**, 107001 (2003)
[8] Y. Okamoto, M. Nohara, H. Aruga-Katori, and H. Takagi, Phys. Rev. Lett. **99**, 137207 (2007)
[9] H. D. Zhou, E. S. Choi, G. Li, L. Balicas, C. R. Wiebe, Y. Qiu, J. R. D. Copley, and J. S. Gardner, Phys. Rev. Lett. **106**, 147204 (2011)
[10] J. G. Cheng, G. Li, L. Balicas, J. S. Zhou, J. B. Goodenough, Cenke Xu, and H. D. Zhou, Phys. Rev. Lett. **107**, 197204 (2011)
[11] B. J. Kim, H. Jin, S. J. Moon, J.-Y. Kim, B.-G. Park, C. S. Leem, J. Yu, T. W. Noh, C. Kim, S.-J. Oh, J.-H. Park, V. Durairaj, G. Cao, and E. Rotenberg, Phys. Rev. Lett. **101**, 076402 (2008)
[12] H. Okabe, M. Isobe, E. Takayama-Muromachi, A. Koda, S. Takeshita, M. Hiraishi, M. Miyazaki, R. Kadono, Y. Miyake, and J. Akimitsu, Phys. Rev. B **83**, 155118 (2011)
[13] R. C. Byrne, and C. W. Moeller, J. Solid State Chem. **2**, 228 (1970)
[14] C. Maunders, J. Etheridge, N. Wright, and H. J. Whitfield, Acta Crystallogr., Sect. B: Struct. Sci. **61**, 154 (2005)
[15] T. Sakamoto, Y. Doi, and Y. Hinatsu, J. Solid State Chem. **179**, 2595 (2006)
[16] See Supplemental Material below
[17] G. Radtke, C. Maunders, A. Saul, S. Lazar, H. J. Whitfield, J. Etheridge, and G. A. Botton, Phys. Rev. B **81**, 085112 (2010)
[18] Y. Singh and P. Gegenwart, Phys. Rev. B **82**, 064412 (2010)
[19] S. Chikara, O. Korneta, W. P. Crummett, L. E. DeLong, P. Schlottmann, and G. Cao, Phys. Rev. B **80**, 140407(R) (2009)
[20] M. A. de Vries, K. V. Kamenev, W. A. Kockelmann, J. Sanchez-Benitez, and A. Harrison, Phys. Rev. Lett. **100**, 157205 (2008)
[21] A. P. Ramirez, S.W. Cheong, and M. L. Kaplan, Phys. Rev. Lett. **72**, 3108 (1994)
[22] S. Nakatsuji, K. Kuga, K. Kimura, R. Satake, N. Katayama, E. Nishibori, H. Sawa, R. Ishii, M. Hagiwara, F. Bridges, T. U. Ito, W. Higemoto, Y. Karaki, M. Halim, A. A. Nugroho, J. A. Rodriguez-Rivera, M. A. Green, C. Broholm, Science **336**, 559 (2012)
[23] O. I. Motrunich, Phys. Rev. B **72**, 045105 (2005)
[24] B. J. Kim, H. Ohsumi, T. Komesu, S. Sakai, T. Morita, H. Takagi, and T. Arima, Science **323**, 1329 (2009)

Supplemental material for "Spin liquid behaviour in $J_{eff} = 1/2$ triangular lattice $Ba_3IrTi_2O_9$"

The XRD refinement of the AP sample is shown in Fig. 5. The crystal parameters obtained from refinement are given in Table I. We have studied the change in the refinement parameters by varying the site disorder of Ir^{4+} ions with Ti^{4+} ions at Ti(2) and Ti(3) sites. The parameters thus obtained are shown in Fig. 6 and Fig. 7. From the figures we can conclude that $(37\pm10)\%$ disorder with Ti(2) site and $(7\pm4)\%$ disorder with Ti(3) site gives best refinement.

ZFC and FC susceptibilities of the AP sample are shown for different fields in Fig. 8.

As mentioned in the main paper, the μ_{eff} and $\mid \theta_{\rm CW} \mid$ values obtained by Bryne *et al.* [13] are much higher than found in our measurements. To find the reason of this mismatch, we have reanalysed the published data on $Ba_3IrTi_2O_9$ in Ref. [13]. The blue open squares in Fig. 9 represent the inverse susceptibility data as published in Ref. [13]. The corresponding susceptibility is shown on the left axis as blue solid squares. We have fitted this susceptibility data with the Curie-Weiss (CW) law in the range $77-363\,$K. This fitting yields temperature independent susceptibility $\chi_{0B} = 3.42\times10^{-4}\,{\rm cm}^3/{\rm mol}$, Curie constant $C = 0.10\,{\rm cm}^3{\rm K}/{\rm mol}$ ($\mu_{eff} = 0.89\mu_B$) and Curie-Weiss temperature $\theta_{\rm CW} = -104\,$K which are somewhat closer to the values obtained from our measurement. Subtracting this χ_{0B}, we have plotted $(\chi-\chi_{0B})^{-1}$ as pink diamonds which is linear in the whole temperature range. Apparently, Bryne *et al.* did not fit their susceptibility data with CW law to find C and χ_0, rather they have chosen a temperature independent susceptibility $\chi_{0A} = 0.50\times10^{-4}\,{\rm cm}^3/{\rm mol}$. We have also shown $(\chi-\chi_{0A})^{-1}$ data points as green solid circles which are much different from $(\chi-\chi_{0B})^{-1}$ data points. The slope corresponding to these green circles has been used by Bryne *et al.* [13] to find $\theta_{\rm CW}$. Further they have used this $\theta_{\rm CW}$ and a single (at 293K) susceptibility data point $(\chi_{\rm M}^{'})$ to get the μ_{eff} from the formula $\mu_{eff} = 2.83\sqrt{\chi_{\rm M}^{'}(T-\theta)}$. Hence, fixing χ_{0A} (without a fitting procedure) and calculating μ_{eff} based on a single susceptibility data point gives unreliable μ_{eff} and $\theta_{\rm CW}$ values in Ref. [13].

Heat capacities for different fields for the AP and QN sample are shown Fig. 10 and Fig. 11, respectively. Schottky fits for different fields for the AP sample are shown in Fig. 12.

In a recent report on $Ba_3CuSb_2O_9$ (space group $P6_3/mmc$), Nakatsuji *et al.* (Ref. [22]) have shown the heat capacity of the system after subtracting the lattice contribution. We term this as $C_{\rm M}^{\prime}$. We have analysed their data to extract magnetic heat capacity ($C_{\rm M}$) after subtracting the Schottky contribution. Inset of Fig. 13 shows $[C_{\rm M}^{\prime}(5\,{\rm T})\text{-}C_{\rm M}^{\prime}(0\,{\rm T})]/T$ and its fit with $f[C_{\rm Sch}(\Delta_1) - C_{\rm Sch}(\Delta_2)]/T$ (see main paper for details).

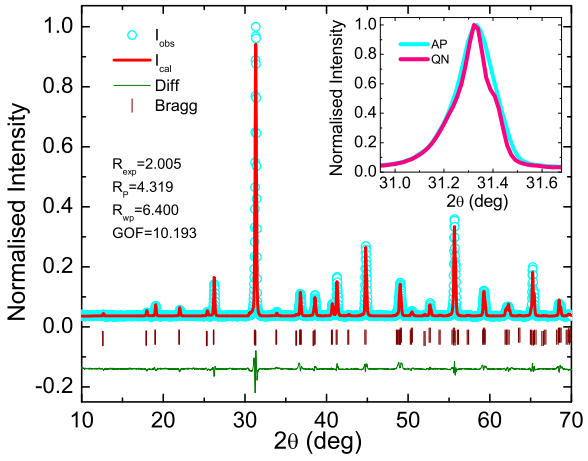

Figure 5: Refinement pattern of as-prepared (AP) $Ba_3IrTi_2O_9$ is shown. Inset: Normalised main peaks for the AP and the quenched sample (QN) are shown.

Table I: Atomic parameters obtained by refining x-ray powder diffraction for as-prepared $Ba_3IrTi_2O_9$ at room temperature with a space group $P6_3mc$.

		x	y	z	g
Ba(1)	2a	0	0	0.24199	1.00
Ba(2)	2b	1/3	2/3	0.07981	1.00
Ba(3)	2b	1/3	2/3	0.39153	1.00
Ir(1)	2b	1/3	2/3	0.64464	0.56
Ti(1)	2b	1/3	2/3	0.64464	0.42
Ti(2)	2b	1/3	2/3	0.83775	0.63
Ir(2)	2b	1/3	2/3	0.83775	0.37
Ti(3)	2a	0	0	0.48763	0.93
Ir(3)	2a	0	0	0.48763	0.07
O(1)	6c	0.16098	0.83898	0.57538	1.00
O(2)	6c	0.48859	0.51138	0.74989	1.00
O(3)	6c	0.16098	0.83898	0.91548	1.00

The fit is good above $\sim 1.5\,$K which means $C_{\rm M}$ is field independent and the field dependence of $C_{\rm M}^{\prime}$ in that region is totally coming from Schottky contribution. Below $\sim 1.5\,$K, the fit deviates from data points indicating field dependence of $C_{\rm M}$. The $\triangle$ obtained from the fit has been used in Eq. 1 of our paper to get the Schottky contribution to heat capacity (f was inferred to be 17%). This is subtracted from $C_{\rm M}^{\prime}$ to get $C_{\rm M}$ for $Ba_3CuSb_2O_9$. For different fields we have extracted $C_{\rm M}$ as shown in Fig. 13. $C_{\rm M}$ is field independent in the range $5-15\,$K and follows a power law with temperature with power 1. Below $\sim 2\,$K $C_{\rm M}$ is field dependent but still follows a power law with power 2.1 for different fields. The behavior is very similar to that found by us in $Ba_3IrTi_2O_9$.

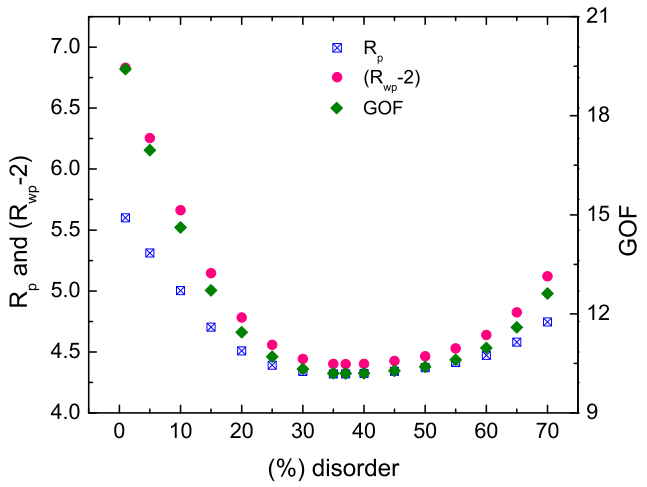

Figure 6: Refinement parameters for the as-prepared (AP) sample obtained by varying disorder at Ti(2) site keeping disorder at Ti(3)site unchanged is shown. R_p and (R_{wp}-2) corresponds to the left axis while goodness of fit (GOF) is plotted on right axis. R_{wp} has been offset downward by 2 to show R_p and R_{wp} on the same axis with clarity.

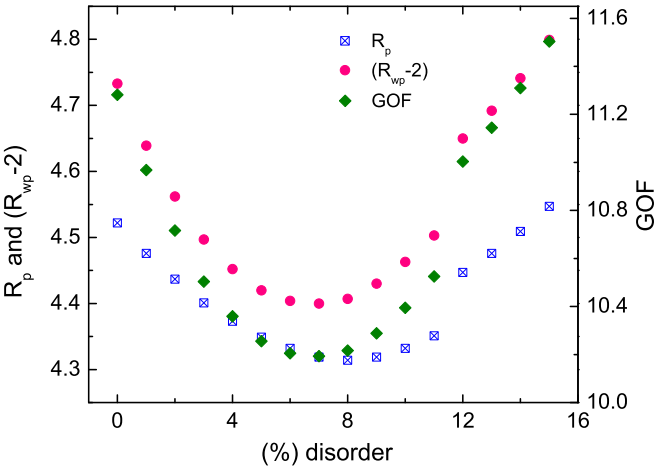

Figure 7: Refinement parameters for the as-prepared (AP) sample obtained by varying disorder at Ti(3) site keeping disorder at Ti(2) site unchanged is shown. R_p and (R_{wp}-2) corresponds to the left axis while goodness of fit (GOF) is plotted on right axis. R_{wp} has been offset downward by 2 to show R_p and R_{wp} on the same axis with clarity.

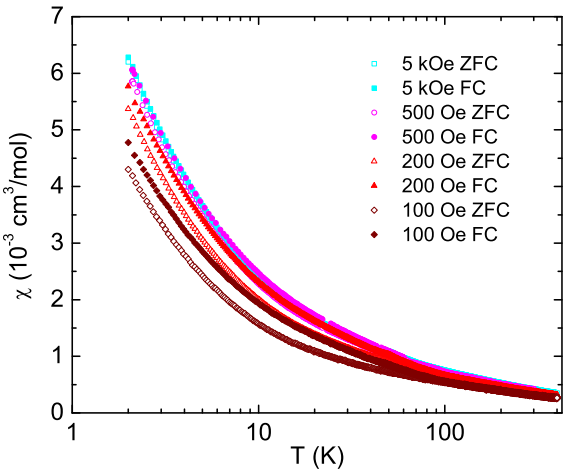

Figure 8: Magnetic susceptibilities of as prepared (AP) $Ba_3IrTi_2O_9$ sample measured at different fields are shown in a semilog scale.

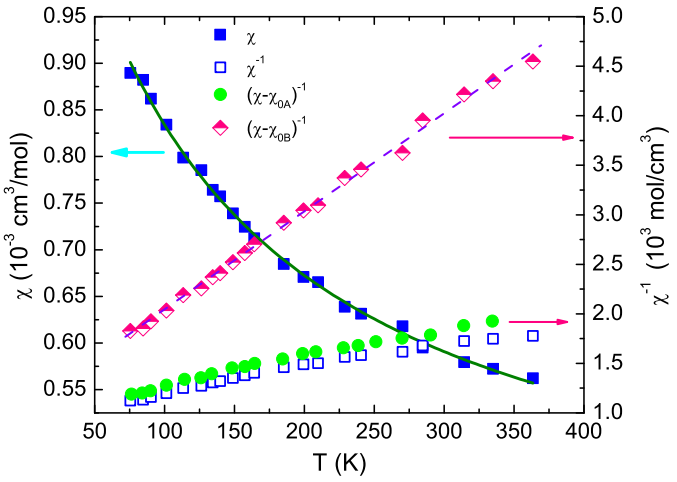

Figure 9: Inverse susceptibility data of $Ba_3IrTi_2O_9$ obtained from Ref. [13] is shown as blue open squares. The corresponding susceptibility is shown as blue solid squares with its fit with Curie Weiss (CW) law (green solid line). Inverse susceptibility after subtracting $\chi_{0A} = 0.5 \times 10^{-4}$ cm^3/mol (as in Ref. [13]) is shown as green solid circles. The inverse susceptibility after subtracting $\chi_{0B} = 3.42 \times 10^{-4}$ cm^3/mol (obtained from CW fit done by us) is also shown as pink diamonds. The dashed line is a guide to eye. Susceptibility is plotted on the left axis while the inverse susceptibilities correspond to the right axis.

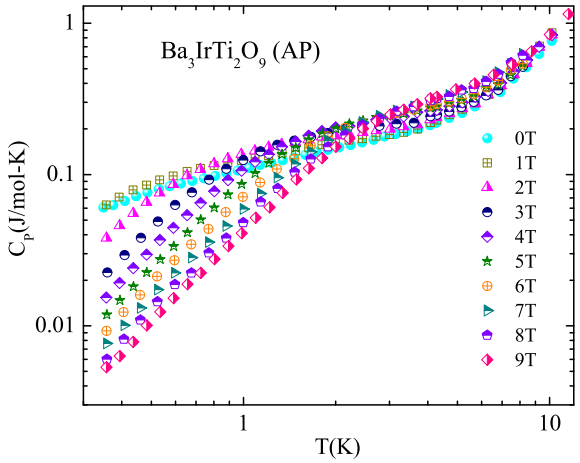

Figure 10: Heat capacities of as prepared (AP) $Ba_3IrTi_2O_9$ sample measured in various applied magnetic fields are shown in a log-log scale.

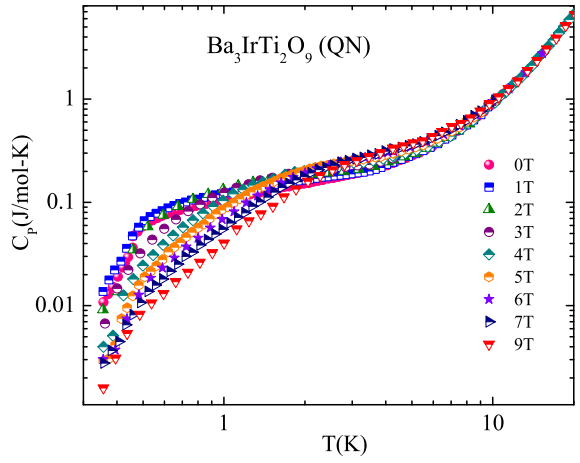

Figure 11: Heat capacities of quenched (QN) $Ba_3IrTi_2O_9$ sample measured in various applied magnetic fields are shown in a log-log scale.

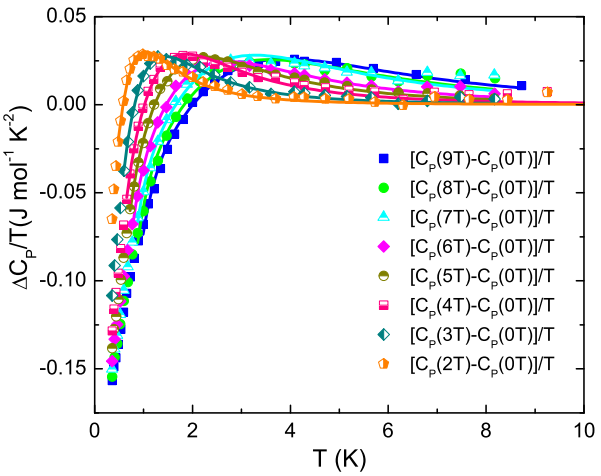

Figure 12: Scattered symbols represent $[C_{\rm P}(\rm n\,T)$-$C_{\rm P}(0\,\rm T)]/T$ of the AP sample and the solid line of corresponding color is the fit (described in the main paper).

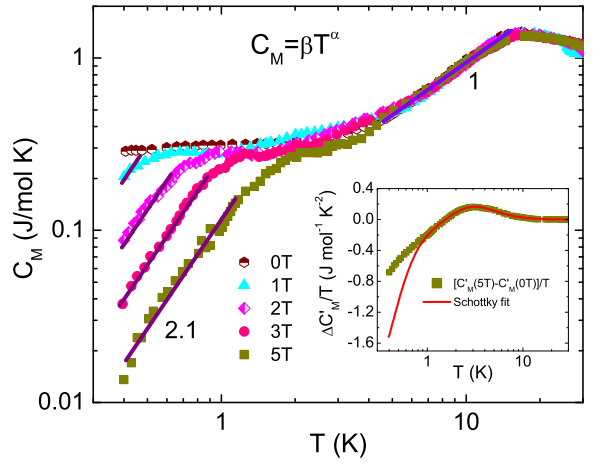

Figure 13: Magnetic heat capacities ($C_{\rm M}$) of $Ba_3CuSb_2O_9$ (taken from Ref. [22]) for different fields after subtracting Schottky contribution are shown. The solid lines are fits to power law. In the low-temperature region $C_{\rm M}$ is field dependent and the power is 2.1 for different fields. In the range $5-15\,\rm K$, $C_{\rm M}$ is independent of field and linear in temperature. Inset: Solid squares represent $[C'_{\rm M}(5\,\rm T)$-$C'_{\rm M}(0\,\rm T)]/T$ and the solid line is the fit (see text).